

Full length article

Non-mechanical optical beam-steering of a liquid crystal laser

Guanxiong Zhang, Steve J. Elston, Andy Schreier, Grahame Faulkner, Atchutananda Surampudi, Dominic O'Brien, Stephen M. Morris^{*}

Department of Engineering Science, University of Oxford, Parks Road, Oxford OX1 3PJ, UK

ARTICLE INFO

Keywords:

Nematic liquid crystals
Chiral nematic liquid crystals
Photonic band-edge
Beam steering
Lasers

ABSTRACT

In this paper, we demonstrate dynamic optical beam-steering of a band-edge chiral nematic liquid crystal (LC) laser that does not involve any change in the configuration of the helical structure. This beam-steering is achieved by exploiting the circular polarisation of the LC laser in combination with tuneable nematic LC phase shifters and fixed polarisation gratings. Experimental results are presented, showing the optical steering of the LC laser emission to four separate discrete spatial positions and, using simulations based on Jones calculus, we explain the appearance and relative intensities of other minor spots that appear around the primary beam. Compared with other approaches of beam-steering an LC laser, this method does not result in an alteration of the laser wavelength, does not change the internal cavity structure of the laser, and has a minimal impact on the intensity of the laser emission. In addition, the whole system (except for the solid-state pump source) is comprised of thin films that are either liquid crystalline or polymers, which provides a tangible route towards a more compact and integrated optically steerable LC laser.

1. Introduction

Dye-doped chiral nematic liquid crystal (LC) lasers have been of considerable interest to the scientific community for two decades since the first realization of band-edge laser emission in 1998 [1,2]. This work demonstrated that coherent monochromatic laser emission could be produced at the edge of a photonic bandgap in accordance with the theoretical work of Dowling [3]. These soft systems provide internally distributed feedback without the use of any mirrors. Such lasers possess a variety of advantages, such as small cavity dimensions, lightweight structures, flexibility and wideband wavelength tuneability [4]. Since the initial studies conducted in the late nineties, research has demonstrated that laser emission can be produced at the edge of the bandgap (band-edge laser) or from a defect mode within the bandgap (defect-mode laser) [3,5]. The unique stimuli-responsive properties of LCs give rise to tuneable laser emission under the influence of a range of external stimuli such as temperature and mechanical stress, as well as optical and electric fields [6,7]. The helical structure of a chiral nematic gives rise to laser emission that is inherently circularly polarised, and the handedness of this circular polarisation depends on the handedness of the chiral nematic helical structure.

Mechanically steering a laser beam away from the original axis of propagation so as to position it at a certain location in space is of interest

for numerous technological applications such as laser micromachining, microscopy and optical wireless communications [8–10]. Conventional mechanical beam-steering approaches that involve the use of prisms and mirrors tend to be large, heavy, and complex [11]. As a result, non-mechanical, optical beam steering is often preferred (and sometimes essential), particularly for applications involving optical communications, navigation, or observation, where power, mass, and volume are primary drivers. Methods that have been developed include LC optical phased arrays [12], solid-state electro-optic modulators [13], and acousto-optic modulators [14]. Furthermore, the ongoing developments of spatial light modulators (SLMs) enable further functionality to be included, such as beam shaping or splitting the beam into multiple directions [15]. However, the use of an SLM is undesirable in some applications because of the cost and size of these systems. Apart from these approaches, researchers have also employed the use of passive [16] and active [17] thin-film LC polarisation gratings to either mechanically [18] or nonmechanically [19] steer infrared laser sources (1064 nm and 1550 nm).

Researchers have also demonstrated methods to steer the beam from LC lasers (both mechanically and nonmechanically). For example, for a band-edge laser, one example involves the engineering of slanted helical structures inside the thin film so that the emission occurs at a steered angle relative to the helical axis [20]. In this work, a periodic

^{*} Corresponding author.

E-mail address: stephen.morris@eng.ox.ac.uk (S.M. Morris).

<https://doi.org/10.1016/j.optlastec.2022.108623>

Received 30 May 2022; Received in revised form 8 August 2022; Accepted 24 August 2022

Available online 23 September 2022

0030-3992/© 2022 The Authors. Published by Elsevier Ltd. This is an open access article under the CC BY license (<http://creativecommons.org/licenses/by/4.0/>).

modulation of the dielectric tensor is introduced along a direction perpendicular to the helical axis using a photoalignment method called “polarisation holography” [21]. The authors achieved a horizontal patterning period of $\Lambda = 620$ nm with a left-handed dye-doped chiral nematic LC sample that had a pitch of $p = 400$ nm (with a half-period of 200 nm), giving rise to a slant angle of $\alpha = \tan^{-1}(p/2\Lambda) \approx 18^\circ$. The tuneability of the emission angle, θ_{lasing} , was found to be in the range between 27.4° and 31.3° with respect to the optical axis. However, by

virtue of the distortion to the helical structure, the wavelength of the LC laser is also inevitably changed alongside the beam-steering process in accordance with the relationship, $\lambda_{\text{lasing}} = 2\Lambda \sin \theta_{\text{lasing}}$.

For defect mode lasers, beam steering has been demonstrated by mechanically bending a defect mode laser that consisted of two polymerised LC thin films separated by a dye-doped polymethylmethacrylate defect layer [5]. In this case, beam-steering of up to 42° with respect to the optical axis was demonstrated by mechanically deforming the device

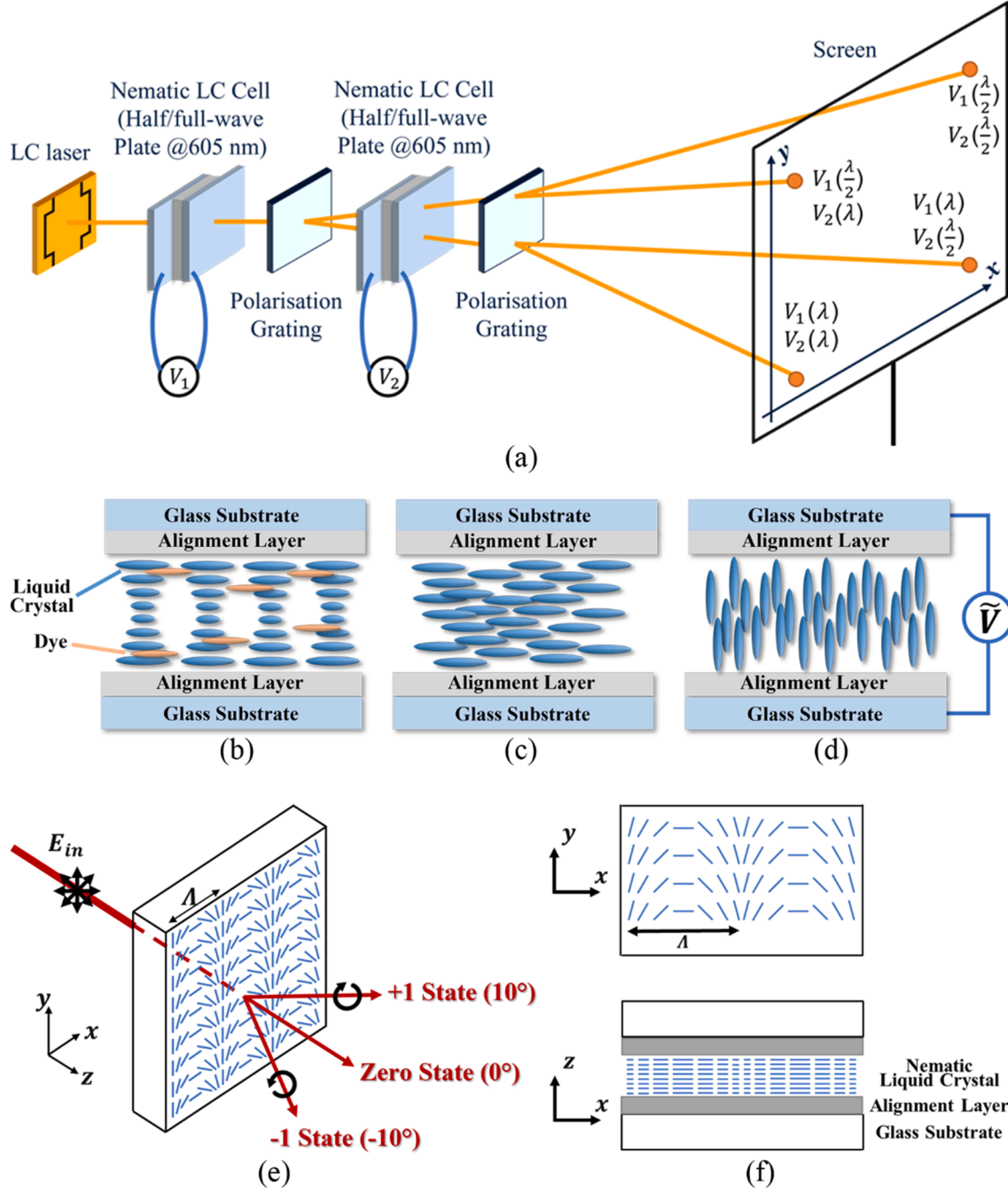


Fig. 1. Optical beam-steering of a liquid crystal (LC) laser (operating at a wavelength of $\lambda = 605$ nm) using tuneable nematic LC phase shifters and static LC polymer polarisation gratings. (a) The system configuration for optically steering an LC laser beam. By applying different voltages to the nematic LC devices so that they function as either half or full-wave plates, the beam can be steered to one of four different spatial locations as illustrated in the figure. V_1 and V_2 are the voltages applied to the first and the second LC cell, respectively. Schematic diagrams of (b) the band-edge LC laser cell (filled with a dye-doped chiral nematic LC), (c) the tuneable nematic LC phase shifters without an electric field and (d) with an electric field. The thickness of the LC laser cell is $8.4 \mu\text{m}$ while the nematic LC cells are $5 \mu\text{m}$. (e) Illustration of the diffraction from the polymerised LC PG with diffraction angles labelled with the corresponding order, and (f) top and side views showing the alignment of the LC director and the device structure, respectively.

so as to vary the radius of curvature of the thin-film from 0 mm to 5 mm. However, it was found that this process of LC laser beam-steering also resulted in an alteration of the laser wavelength together with a shift in the defect mode. In previous demonstrations, it is also likely that the emission intensity/efficiency was degraded during the process of beam-steering, although this was not discussed specifically.

In this paper, a non-mechanical method of steering an LC laser beam is demonstrated that takes place without deforming the LC macroscopic structure/device architecture nor change the laser wavelength or other emission characteristics such as the excitation threshold, slope efficiency etc. This is achieved by adjusting the polarisation state of the LC laser using voltage tuneable nematic LC devices and then steering the beam according to its current polarisation state by diffraction from polarisation gratings (PGs). This approach to nonmechanical beam-steering is based upon the concept proposed by Jihwan Kim et al [16,19]. PGs are particularly interesting for non-mechanical beam-steering systems because they are lightweight, compact, low-power, and inexpensive [11]. They combine numerous advantageous properties including a near-ideal diffraction efficiency of close to 100% and strong polarisation sensitivity in terms of the ± 1 states. These properties make PGs effective tools in spectral ellipsometers [22] and snapshot imaging polarimeters [23]. In addition, PGs have a wide range of other applications, such as in spatial heterodyne interferometers [24] and wavelength selective switches [25]. Research has also shown that PGs can be potentially used as polarisation-based multiplexers and demultiplexers, a light modulator, or a polarizing beam splitter in optical data transmitting communication systems [26].

An illustration of the beam-steering concept and configuration is shown in Fig. 1. In this work, we demonstrate optical beam-steering of an LC laser both in the horizontal and vertical directions, but in principle, additional discrete positions can be obtained by adding extra tuneable phase shifters and PGs, in accordance with the work of Jihwan Kim et al [16,19,27]. The steering of the beam takes place with minimal impact on the intensity of the laser beam because there is no change to the helical structure of the chiral nematic LC. Results are presented that reveal the appearance of some other spots, which are of much lower intensities, surrounding the primary beam during the steering process. The formation of these spots is explained with the support of numerical simulations based on Jones matrices.

2. Calibration and simulation of the PGs

The PGs used in the following experiments were sourced from Edmund Optics. They are designed for operation at a centre wavelength of 550 nm, and the retardance is π at this wavelength. These gratings are 0.45 ± 0.04 mm thick and 25.00×25.00 mm ± 0.25 mm in dimension with 286 grooves per millimetre. The diffraction angle and minimum diffraction efficiency are quoted as being 10° and 96%, respectively, resulting in a maximum of 4% light leakage into the zero-order (without being steered) regardless of the polarisation state of the incident light. The substrate of the PG is D263 glass with an anti-reflective coating. The nematic LC cells used in this work function as continuously variable retarders, which are fabricated by capillary filling the nematic LC mixture, E7 (Synthon Chemicals Ltd), into commercially available 5 μ m thick anti-parallel rubbed glass cells (LC-2, Instec) that are coated with indium-tin-oxide (ITO) electrodes and polyimide alignment layers.

For this work, PGs were employed to give rise to diffraction that is dependent on the polarisation state of the incident light source. PGs steer the beam to the +1 order and/or -1 order depending upon the polarisation states of the incident light, with diffraction angle of 10° and -10° , respectively. For example, unpolarised light is diffracted evenly between the +1 and -1 orders while circularly polarised light is diffracted entirely to one specific order, depending upon the handedness of the polarisation. For convenience, the -1 state is defined as the diffraction state for left circularly polarised light, while the +1 state is defined as that for right circularly polarised light. By switching the

handedness of the incident light, two PGs placed with their axes aligned orthogonally can steer the beam to one of four quadrants depending upon the input polarisation state at each PG.

A continuous-wave Helium-Neon (He-Ne) laser (05-LGP-193, Melles Griot) with an emission wavelength at 543.5 nm was used to initially characterise the PGs. First, the polarisation of the He-Ne laser was converted to be right circularly polarised by a combination of a polariser and a quarter-wave plate (at 546 nm). A CCD camera (DCU224C, Thorlabs) was used to capture the diffraction pattern on a screen placed in the far-field away from the PGs. The results of this characterisation are presented in Fig. S1 in the [Supplementary Information](#).

Besides the primary beam, which is diffracted to different spatial locations, other minor spots are observed, which are significantly lower in intensity compared with the main beam. These additional spots, which also have been observed by other researchers [19,27], can be divided into three categories: zero-order, sub-order, and opposite-order spots. The zero-order spots are non-diffracted spots (with zero diffraction angle) that appear at the zero position in the x and y-coordinates defined in this work. In addition to the inherent zero-order leakage that occurs due to imperfections in the PG mentioned earlier, a mismatch in the wavelength between the emission wavelength of the laser and the design wavelength of the PG is another reason for the appearance of the zero-order spot. Specifically, the retardance of a PG, ϕ_p , is expected to be given by $\phi_p = 543.5\pi/550$ when working with the He-Ne laser. The spots that are surrounding the primary beam with much weaker intensities, on the other hand, are defined as sub-order spots. The diffraction angles of these spots are at $\pm 5^\circ$ and $\pm 15^\circ$, which is equal to one half or 1.5 times the designed diffraction angle of the PG. The appearance of these spots is assumed to be caused by a slightly asymmetrical periodic structure of the PGs. For the so-called opposite-order spots, with the opposite diffraction angle to the primary beam, they possess the opposite polarisation state to that of the primary beam. There are two reasons why opposite-order state spots might appear: one reason could be that there is a slight residual birefringence introduced by the PG substrates and the other reason is that the incident light does not have an ideal circular polarisation state. All these characteristics can be accounted for with simulations carried out based upon Jones matrices (*vide infra*). A recent report used a combination of elastic continuum theory of LCs and Jones matrices to simulate the behaviour for light that was at oblique incidence to a series of cascaded PGs [28]. Here we use a simpler approach to simulate and explain light propagation through a combination of LC cells and PGs as well as the appearance of each spot due to diffraction.

The Jones matrix for the PG can be determined by regarding it as a general retarder with an arbitrary fast axis at an angle [23,29] θ_p and a retardance of ϕ_p such that.

$$J_p = \begin{bmatrix} \cos^2\theta_p + e^{i\phi_p}\sin^2\theta_p & (1 - e^{i\phi_p})\cos\theta_p\sin\theta_p \\ (1 - e^{i\phi_p})\cos\theta_p\sin\theta_p & e^{i\phi_p}\cos^2\theta_p + \sin^2\theta_p \end{bmatrix} \quad (1)$$

If the periodicity of the PG is along the x-axis and is given by Λ , and the light is propagating along the z-axis, then the angle θ_p can be expressed as.

$$\theta_p = 2\pi x/\Lambda \quad (2)$$

Similarly, the Jones matrix for a nematic LC cell functioning as a tuneable wave plate can be expressed as.

$$J_N = \begin{bmatrix} \cos^2\theta_N + e^{i\phi_N}\sin^2\theta_N & (1 - e^{i\phi_N})\cos\theta_N\sin\theta_N \\ (1 - e^{i\phi_N})\cos\theta_N\sin\theta_N & e^{i\phi_N}\cos^2\theta_N + \sin^2\theta_N \end{bmatrix} \quad (3)$$

where θ_N is the orientation angle of the fast axis with respect to the x-axis, and ϕ_N is the retardance of the LC wave plate introduced between the fast and slow axes.

Given that the Fresnel number for PG diffraction satisfies the condition for the Fresnel number, $F \gg 1$ (the radius of the laser beam at the PG is of the order of 0.1 mm, and the distance of the screen from the PG

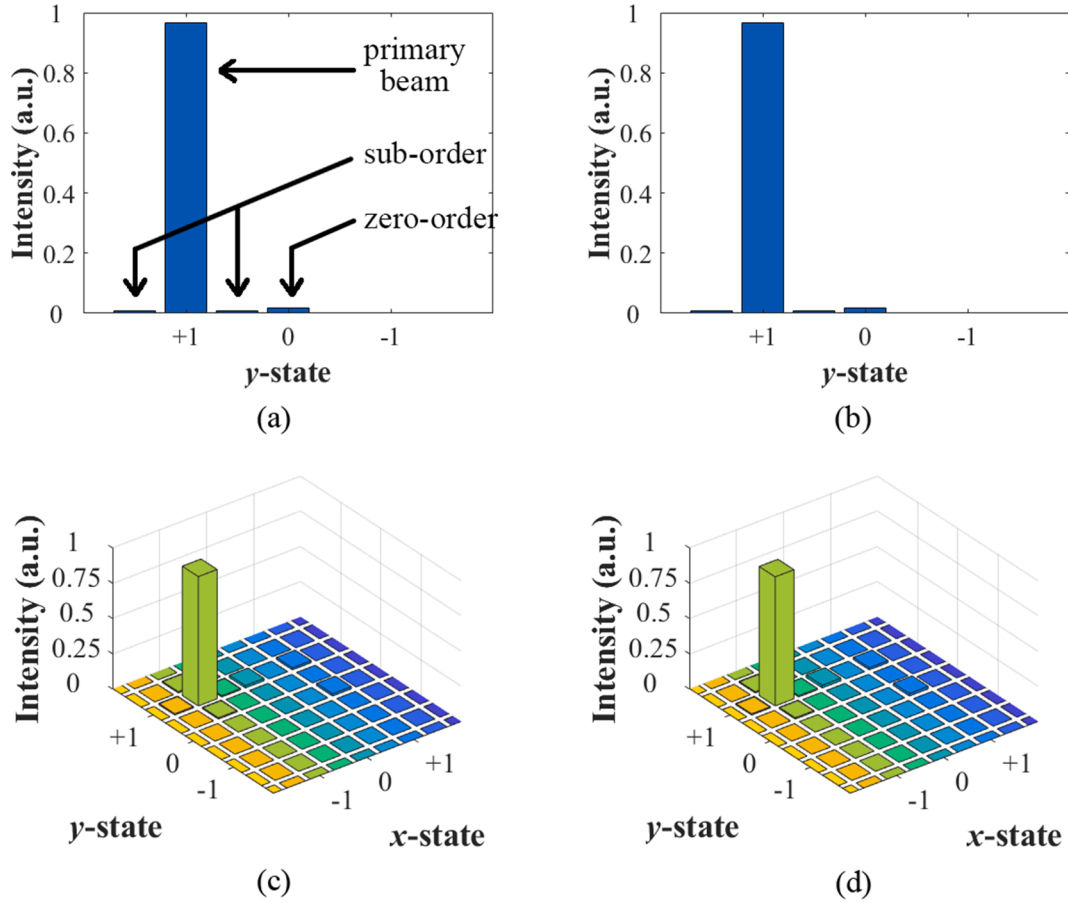


Fig. 2. Simulation and experimental results for the relative intensity of each spot observed (primary beam, zero-order, sub-order spots) in the far-field pattern for both one and two-dimensional beam-steering. (a) Simulation result for one-dimensional beam-steering and the corresponding (b) experimental result for one-dimensional beam-steering using a single PG. (c) Simulation result for two-dimensional beam-steering and (d) the corresponding experimental result for two-dimensional beam-steering.

is of the order of 10 cm), the propagating beam can be described in terms of far-field Fraunhofer diffraction. Therefore, light incident on the screen is simply the Fourier transform of the aperture (PG) distribution. To investigate the slight asymmetrical periodic structure of the PGs, each birefringence period Λ is divided into two parts with unequal lengths $k\Lambda$ and $(1-k)\Lambda$, where k is a constant parameter less than 0.5. The fast axis angle θ_p rotates by π within $k\Lambda$ and $(1-k)\Lambda$, respectively. That is, in each birefringence period, the angle θ_p takes the form.

$$\theta_p = \begin{cases} \pi x/k\Lambda, & x \leq k\Lambda \\ \pi + \pi(x-k\Lambda)/(1-k)\Lambda, & k\Lambda < x \leq \Lambda \end{cases} \quad (4)$$

Using Equations (1) - (4), simulations and measurements for one and two-dimensional beam-steering of the He-Ne laser with the PGs were carried out and the relative intensities for each spot are shown in Fig. 2. The laser spot intensities were measured using a photodiode (PDA36A-EC, Thorlabs) connected to an oscilloscope (TBS1052C, Tektronix). Fig. 2(a) and (b) are the simulation and experimental results for one-dimensional beam-steering. The primary beam appears at the +1 state while minor sub-order spots are observed at the (0, +0.5) position and (0, +1.5) position. There is also a zero-order at the centre in Fig. 2(b), which can be considered to be entirely from intrinsic zero-order leakage with a value of 1.6% of the total incident power. Similarly, Fig. 2(c) and (d) are the simulation and experimental results for two-dimensional beam-steering, where the primary beam is located at the (-1, +1) position surrounded by four minor sub-order spots. Two spots are found at the (0, +1) and (+1, 0) positions as well as an opposite-order spot at the (+1, +1) position. The primary beam has a relative intensity of 0.91

while that of the zero-order spot at (0, +1) is 0.02 which is the highest of all the spots excluding the primary beam. This result is similar to that found in another study that employed a ray-tracing tool to simulate two-dimensional beam-steering achieved by a 1550 nm laser and corresponding PGs [27]. The main spot had a relative power of 87% of the total power and any of the highest intensity single side spots were still lower than 1.5% of the total power (these side spots were claimed to be caused mainly by the zero-order leakage of the PGs).

The value of the asymmetrical period parameter k and the additional residual birefringence introduced by the PG substrates can be estimated by adjusting their values so that the simulation results are close to the experimental measurements. Specifically, it was found that the simulations closely matched the experiments when the asymmetrical period parameter k was set to 0.46 and the additional residual birefringence introduced by the PG substrates was set to 0.05π . The similarity between Fig. 2(a) and (b), together with Fig. 2(c) and (d) suggests that the asymmetrical periodic structure of the PG results could indeed be the reason for the appearance of the sub-order spots and that residual birefringence of the substrates gives rise to spots with the opposite handedness polarisation on the screen. In most previous reports the focus has been on the investigation of the first and zeroth order spots [27,30,31], while this work also presents an explanation for the appearance of sub-order and opposite-order spots.

3. Optical beam-steering of a liquid crystal laser

The LC laser used in this study used a dye-doped chiral nematic LC mixture: E7 + 2.5 wt.% chiral dopant (R5011) + 1 wt.% of the laser dye

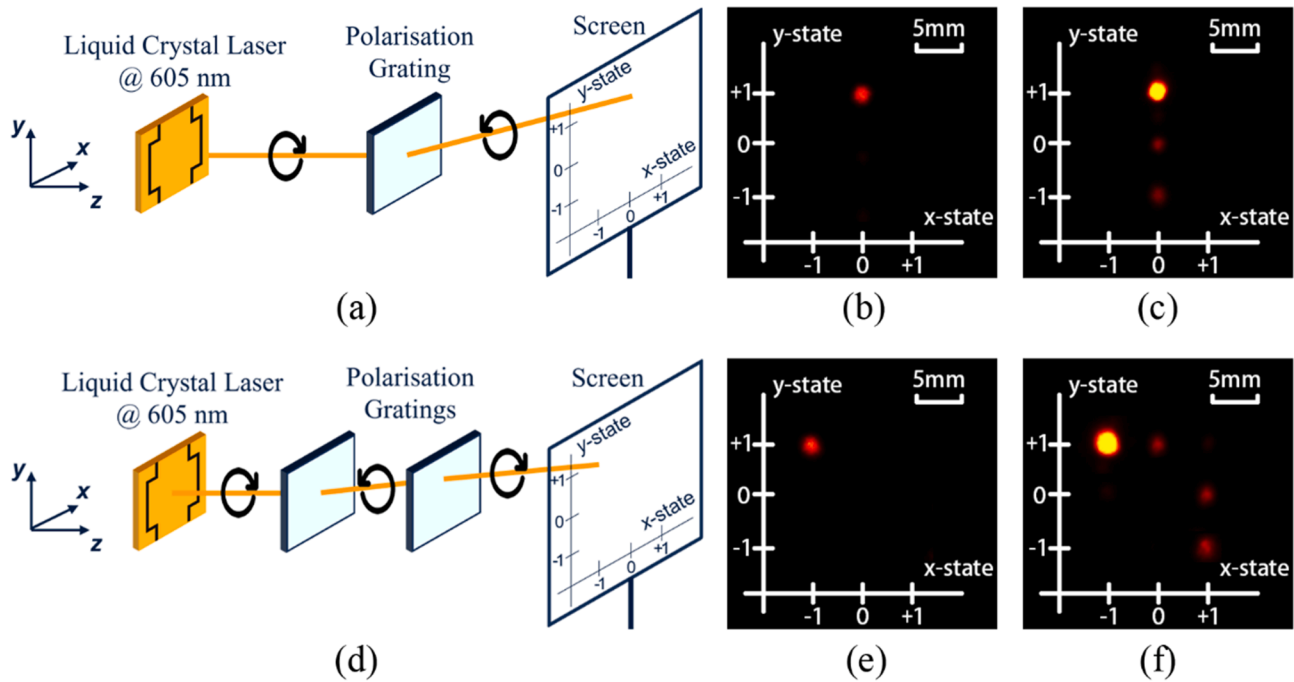


Fig. 3. Demonstration of (a) one-dimensional beam-steering of an LC laser using one PG and (b) the corresponding diffraction pattern recorded on the screen. (c) The primary beam is allowed to saturate the camera so that the other spots can be seen on the screen. Demonstration of (d) two-dimensional beam-steering of an LC laser using two PGs placed with their axes orthogonal to one another and (e) the corresponding diffraction pattern observed on the screen. (f) The primary beam saturated the camera in order to see the other weaker intensity spots on the screen. The thickness of the LC layer was $8.4\ \mu\text{m}$ while the measurement temperature was $25\ ^\circ\text{C}$.

4-(Dicyanomethylene)-2-methyl-6-(4-dimethylaminostyryl)-4H-pyran (DCM). E7 is a well-known nematic LC mixture (Synthon Chemicals Ltd), R5011 is a right-handed chiral dopant (Merck KGaA), and DCM (Exciton) is a commonly used laser dye with a typical lifetime in an LC host of 2 ns and a quantum efficiency of 45% [32]. The concentration of the chiral dopant was chosen so that the long-wavelength band-edge approximately coincided with the gain maximum of the DCM laser dye. The mixture was then capillary filled into a glass cell with anti-parallel rubbed polyimide alignment layers and spacer beads dispersed in the glue walls that resulted in a cell gap of $8.4\ \mu\text{m}$. The optical pump source for this LC laser was a solid-state frequency-doubled Nd:YAG laser (6FTSS355-Q4-S, CryLas) with a wavelength of $\lambda = 532\ \text{nm}$ and a pulse length of 1 ns. The emission energy of the pump beam was controlled using a manually controlled neutral density filter. To minimise photobleaching of the sample [33], the repetition frequency was set to 10 Hz. The Nd:YAG laser output was converted to left-handed circularly polarised light by a combination of a polariser and a quarter-wave plate. This laser beam was used to excite the dye-doped chiral nematic LC cell to produce an LC laser output with a near right-handed circular polarisation state, which was then collected by a microscope objective (magnification: $4\times$, numerical aperture: 0.1). The 532 nm pump laser radiation was removed from the detection system using a long-pass filter.

The LC laser had a wavelength of $\lambda = 605.1\ \text{nm}$ and an excitation threshold of $E_{\text{th}} = 671.9\ \mu\text{J}/\text{cm}^2/\text{pulse}$. This was smaller than the typical values of $\sim 1\ \text{mJ}/\text{cm}^2/\text{pulse}$ often reported in the literature [32], which is considered to be due to the shorter pulse length of the Nd:YAG laser used in this work. Previous research has shown that pump lasers with shorter pulse lengths tend to lead to lower excitation thresholds of the LC laser [34]. Results for the characterisation of the LC laser, in terms of the emission wavelength and the excitation threshold, are presented in Fig. S2 in the Supplementary Information.

When only one PG is placed in the system, the LC laser with right-handed circular polarisation is steered vertically upwards to the (0, +1) position. The experimental configuration and the far-field pattern observed on the screen are shown in Fig. 3(a) and (b), respectively. Fig. 3

(c) shows an example image captured with a higher intensity input so that the zero-order and opposite-order spots can be clearly seen. Compared to the beam-steering results obtained for the He-Ne laser, this LC laser produces a slightly stronger zero-order spot because of the larger wavelength mismatch ($\lambda = 605\ \text{nm}$ for the LC laser compared with the design wavelength of the PG of $\lambda = 550\ \text{nm}$). In addition, the opposite-order spot for this LC laser in Fig. 3(c) also possesses a higher relative intensity compared with that observed for the circularly polarised He-Ne laser in Fig. S1(c), which indicates that the residual birefringence of the PG substrates is not the only reason for the appearance of the opposite-order spots. Instead, the incident laser is not purely circularly polarised. From a theoretical perspective, it is expected that the emission at the band-edge of a dye-doped chiral nematic LC should be circularly polarised. However, recent studies have also presented evidence that might indicate that these LC lasers are not purely circularly polarised, but instead are very close to a circularly polarised source with the same handedness as the helical structure [35,36].

When a second identical PG is added into the system, the configuration and spot pattern are shown in Fig. 3(d) and (e). Fig. 3(f) is another example of an over-exposed image to demonstrate the appearance of the secondary lower-intensity spots. The primary beam at (0, +1) in Fig. 3(c) exhibits a right-handed circular polarisation state before diffraction and is nearly left-handed circularly polarised after the diffraction from the first PG (with a phase delay of $605\pi/550$ introduced by the PG). Consequently, the diffraction by the second PG steers it to (-1, +1) leaving a zero-order spot at (0, +1) due to the wavelength mismatch. The other two spots in Fig. 3(f), at (+1, 0) and (+1, -1), are correspondingly diffracted from the two spots in Fig. 3(c), at (0, 0) and (0, -1), respectively.

Since the LC laser is not purely circularly polarised, it is simulated by an elliptically polarised source with an initial phase difference of 0.3π between the x and y components of the electric field vectors. The simulation results for one- and two-dimensional beam-steering of an LC laser are shown in Fig. 4(a) and (c), respectively. The location and corresponding intensities of the primary beam, zero-order and opposite-order spots are labelled in Fig. 4(a). These simulation results are in good

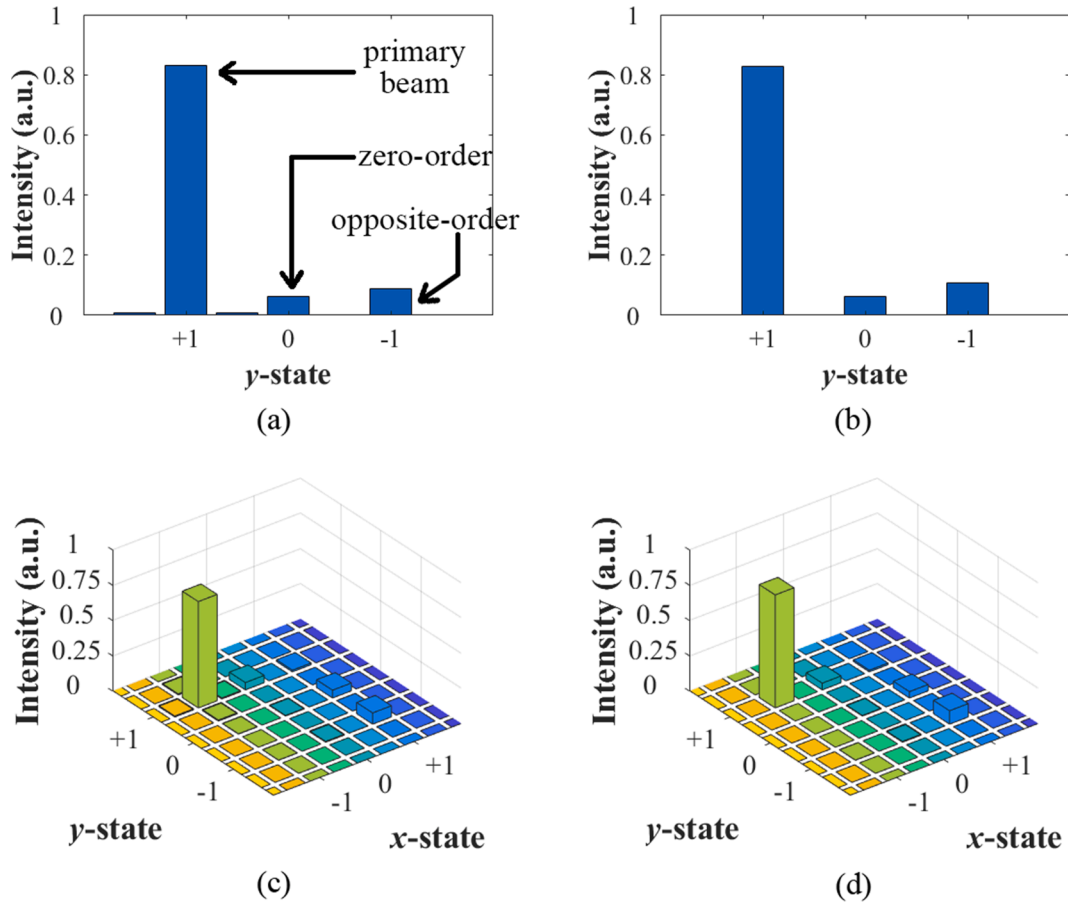


Fig. 4. Simulation and experimental results for the relative intensity of each spot observed in the far-field when steering emission from the LC laser. (a) Simulation results for one-dimensional beam-steering and (b) the corresponding experimental results for one-dimensional beam-steering. (c) Simulation results for two-dimensional beam-steering and (d) the corresponding experimental results for two-dimensional beam-steering.

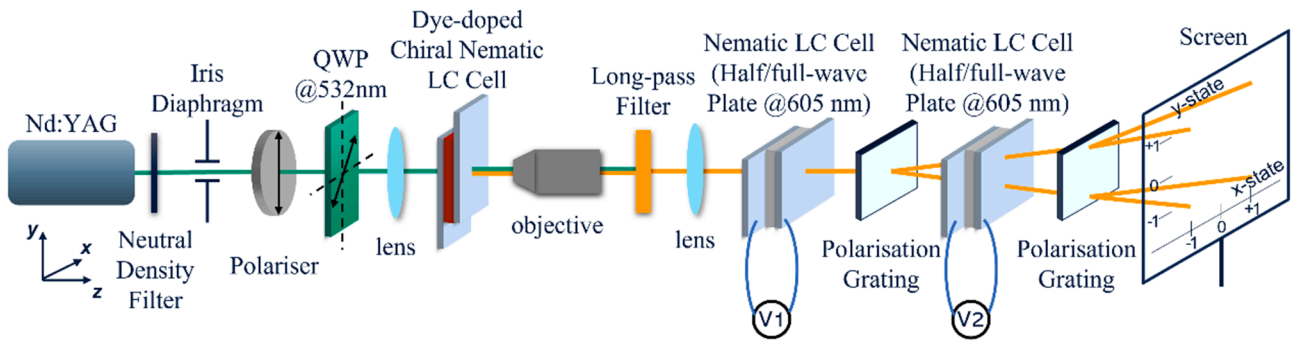
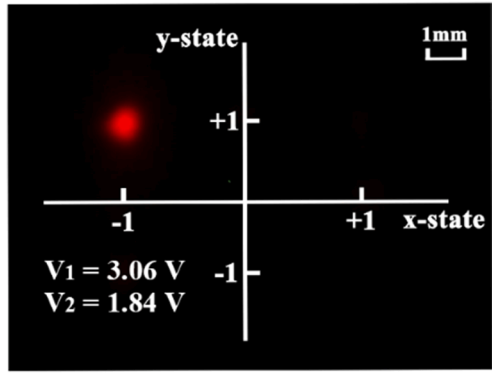


Fig. 5. The experimental system used to demonstrate dynamic optical beam-steering of an LC laser. QWP: quarter-wave plate; HWP: half-wave plate; FWP: full-wave plate; V_1 : the voltage applied to the first nematic LC cell; V_2 : the voltage applied to the second nematic LC cell.

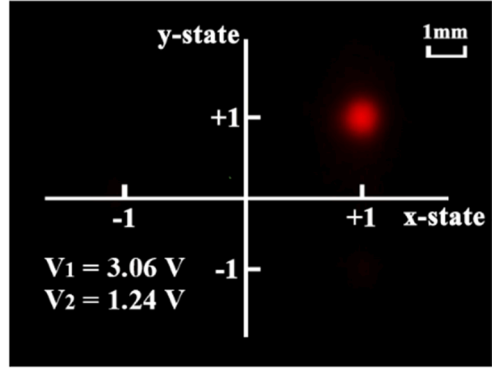
agreement with the experimental results as shown in Fig. 4(b) and (d). This demonstrates the validity of the Jones matrix simulation as well as the modelling of the LC laser and the PGs.

The next step is to demonstrate dynamic steering of the LC laser to any one of four spatial locations $(-1, +1)$, $(+1, +1)$, $(+1, -1)$, and $(-1, -1)$ through the introduction of tuneable nematic LC wave plates in accordance with previous studies [16,19,27]. The experimental configuration used in this study to dynamically steer the beam is illustrated in Fig. 5. The Nd:YAG laser produces a pulsed laser output with a frequency of 10 Hz, which is converted by a polariser and a quarter-wave plate to left-handed circularly polarised light. This laser beam excites the dye-doped chiral nematic LC cell to produce an LC laser output with a

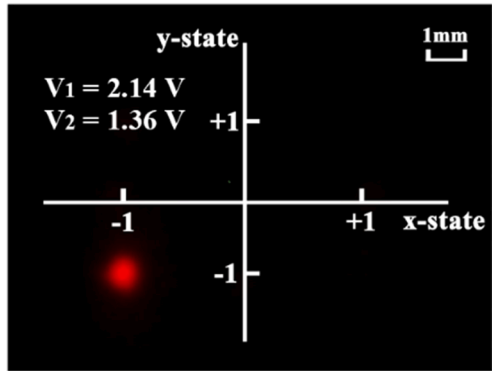
near right-handed circularly polarisation state, which is collected by the objective and lens. The Nd:YAG laser is filtered by a long-pass filter. By changing the voltage V_1 on the first nematic LC cell, it can be used as a half-wave plate or full-wave plate at $\lambda = 605$ nm. If the first nematic LC cell acts as a full-wave plate, the LC laser polarisation state is maintained, and is diffracted to the $+1$ state (in the y-direction) by the first PG. When the nematic LC is used as a half-wave plate, on the other hand, the LC laser is reversed to the opposite handedness, which is then diffracted to the -1 state (in the y-direction). In the same way, the second nematic LC cell can also maintain or change the handedness of the LC laser by controlling the magnitude of the voltage V_2 , so as to switch the beam steering direction between the $+1$ state (x-direction) and the -1



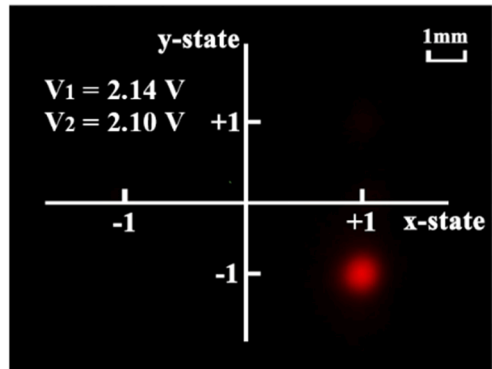
(a)



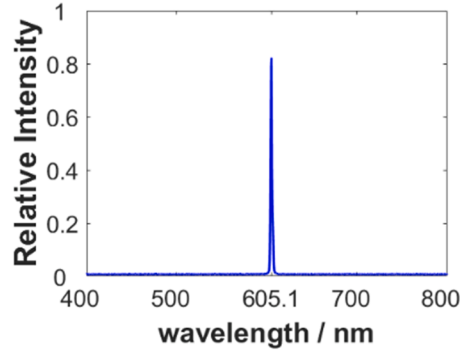
(c)



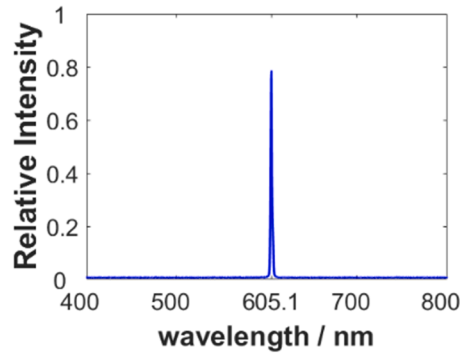
(e)



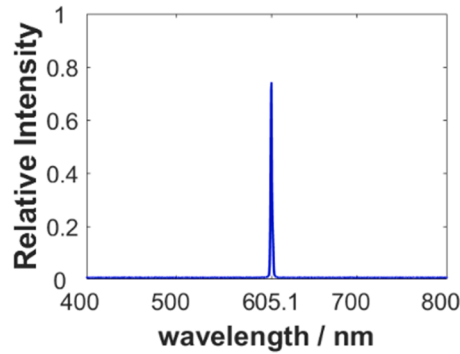
(g)



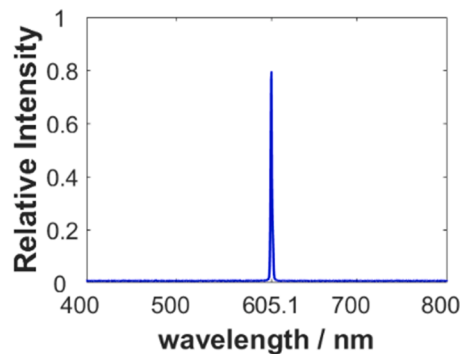
(b)



(d)



(f)



(h)

Fig. 6. Experimental results demonstrating non-mechanical LC laser beam-steering. The thickness of the LC layer in the laser cell was 8.4 μm , which was optically pumped by an Nd:YAG laser with a repetition rate of 10 Hz. The thicknesses of the nematic LC layers used as tuneable wave plates were 5 μm and were driven by a 1 kHz square-wave electric field. By applying the appropriate voltage amplitudes, the LC laser beam was steered to (a) top-left (-1, +1), (b) top-right (+1, +1), (c) bottom-left (-1, -1), or (d) bottom-right (+1, -1). The voltages applied to the nematic LC cells are overlaid on the photographs in (a), (c), (e), and (g). The emission spectrum next to each diffraction pattern demonstrates the relative intensity (with respect to the original laser beam) and the wavelength of the steered laser beam.

Table 1

Wavelength of the primary beam and relative intensities of each spot when the LC cells were subjected to different voltages to switch between the full-wave plate and half-wave plate conditions.

Voltages for nematic LC cells		Location of the primary beam	Wavelength of the primary beam	Relative intensities for each spot			
Cell 1	Cell 2			(-1, +1)	(+1, +1)	(-1, -1)	(+1, -1)
3.06 V	1.84 V	(-1, +1)	605.1 nm	1	0.077	0.084	0.057
3.06 V	1.24 V	(+1, +1)	605.1 nm	0.080	1	0.043	0.088
2.14 V	1.36 V	(-1, -1)	605.1 nm	0.094	0.048	1	0.080
2.14 V	2.10 V	(+1, -1)	605.1 nm	0.079	0.057	0.050	1

state (x-direction). The combination of the two PGs and two nematic LC devices means that the beam can be switched from say the (+1, +1) position to the (-1, -1) position by changing the wave plate conditions of the nematic LC devices.

The voltages at which the nematic LC cell behaves as a half-wave plate or full-wave plate are specified by initially removing the second set of the nematic LC cell and PG from the system leaving only one nematic LC cell and one PG to steer the beam in the vertical direction. When the voltage applied to the first nematic LC cell was 3.06 V, the top diffracted spot at (0, +1) reaches its maximum intensity (measured by the same photodiode as before) suggesting that the nematic LC cell is now working as a full-wave plate. Alternatively, when the applied voltage is set to 2.14 V, the laser beam is steered to the bottom position at (0, -1) with maximum intensity. Thus, the first nematic LC cell behaves as a half-wave plate when this voltage amplitude is applied.

Subsequently, the second nematic LC cell and PG in Fig. 5 were placed back in the system. When V_1 (the voltage applied to the first LC cell) was equal to 3.06 V and by adjusting the value of V_2 (the voltage applied to the second LC cell) to be either 1.84 V or 1.24 V, the LC laser beam can be steered either to the top-left (-1, +1) or top-right (+1, +1) quadrants, respectively, with the highest intensities. Alternatively, setting $V_1 = 2.14$ V, the LC laser beam can then be steered to either the bottom-left (-1, -1) or bottom-right (+1, -1) quadrants when V_2 was set to either 1.36 V or 2.10 V, respectively. Note that the variation in voltages is caused by different cell thicknesses due to manufacturing variation and different incident angles due to the action of the first PG. The second LC cell needs to provide different birefringence offsets for different beam-steering directions with small voltage differences to modulate the diffracted primary beam to circular polarisation.

The four sets of voltages that were applied to the nematic LC cells demonstrate the operating principle of the device whereby the primary beam is steered to one of four different spatial directions. When the nematic LC cells are subjected to voltages that do not match these conditions, the LC cells no longer behave as half/full-wave plates and therefore the intensity of the primary beam reduces, and the opposite order spots will appear as the LC laser beam will not be circularly polarised. As the difference between the actual applied voltage and the required voltage increases, the brightness of the opposite order spots increases.

The photographs in Fig. 6 demonstrate that the beam is successfully steered to four separate directions when the appropriate voltages were applied to the nematic LC cells. A video of the demonstration of the LC laser beam steering can be found in [Supplementary Movie 1](#). Unlike other LC laser beam-steering approaches [5,20,37] where the laser wavelength changes with the structural variation of the LC laser, this method of LC laser beam-steering does not change the wavelength. A spectrometer (USB2000+, Ocean Optics) was used to measure the spectrum of the steered beam at each of the four separate locations and these are shown in Fig. 5(b)(d)(f)(h). The wavelength of the laser remained at $\lambda = 605.1$ nm regardless of the steering direction.

The overall response time of the system was measured to be 170 ms when the voltage applied to the second LC cell was switched from 1.24 V to 1.84 V, which causes the beam to be steered from the top-left (-1, +1) location to the top-right (+1, +1) position. The response time for the switching between the other locations was found to be shorter since

higher applied voltages are required. The measurement method and results are presented in Fig. S3 in the [Supplementary Information](#). For further potential applications that require shorter response times, for instance, in optical communications and light detection and ranging (LiDAR), thinner LC cells and higher voltages can be implemented so that the cells are working as zero-order half/full-wave plates. Previous work has shown that the response time for nematic LCs can be as low as a few milliseconds when the material and cell thicknesses are carefully selected [38].

The results for the corresponding relative intensities and drive voltages required are presented in Table 1. The relative intensity of each spot in the four spatial quadrants with respect to the primary beam was evaluated by dividing the measured intensity of each spot by the highest intensity value among the four spots. Even though additional beams appear, the intensities of these 'residual' spots at the other three locations are less than a tenth of the intensity of the primary beam. Therefore, for most potential applications such as in optical communications and LiDAR, these additional beams would have little influence on the resulting performance of the beam-steering system.

4. Conclusions

In summary, optical beam steering of a band-edge LC laser which does not involve changes to the helical structure and consequently changes to the emission wavelength and intensity has been demonstrated. The entire configuration (except for the Nd:YAG pump laser) is liquid crystal-polymer-based and electrical-controlled, which provides a potential route toward a more compact configuration in the future. A technique that allows imperfections in the polarisation grating structure to be modelled has been developed, which matches the experimental results and measurements. Multiple spots appeared in the far-field along with the primary beam with intensities lower than 10% of the desired beam, however, this is not an issue for many applications. The findings presented in the paper are supported by the results from simulations using Jones matrices and the principle of far-field Fraunhofer diffraction. The combination of this all-LC system comprising an LC laser, tuneable LC waveplates, and LC PGs provides a route towards a very compact system that could be deployed as a complete laser source-beam steering system for potential use in optical communications, navigation and tracking, and LiDAR applications.

CRediT authorship contribution statement

Guanxiong Zhang: Conceptualization, Validation, Investigation, Data curation, Writing – original draft. **Steve J. Elston:** Conceptualization, Methodology, Investigation, Supervision, Writing – review & editing. **Andy Schreier:** Validation, Investigation, Writing – review & editing, Methodology. **Grahame Faulkner:** Validation, Investigation, Writing – review & editing, Methodology. **Atchutananda Surampudi:** Writing – review & editing, Methodology. **Dominic O'Brien:** Conceptualization, Methodology, Investigation, Writing – review & editing, Project administration, Funding acquisition. **Stephen M. Morris:** Supervision, Conceptualization, Project administration, Funding acquisition, Writing – review & editing.

Declaration of Competing Interest

The authors declare that they have no known competing financial interests or personal relationships that could have appeared to influence the work reported in this paper.

Data availability

Data will be made available on request.

Acknowledgements

Atchutananda Surampudi gratefully acknowledges the Commonwealth Scholarship Commission (UK) for support through a Commonwealth Doctoral Scholarship.

Appendix A. Supplementary material

Supplementary data to this article can be found online at <https://doi.org/10.1016/j.optlastec.2022.108623>.

References

- [1] V.I. Kopp, B. Fan, H.K.M. Vithana, A.Z. Genack, Low-threshold lasing at the edge of a photonic stop band in cholesteric liquid crystals, *Opt. Lett.* 23 (1998) 1707, <https://doi.org/10.1364/OL.23.001707>.
- [2] H. Finkelmann, S.T. Kim, A. Muñoz, P. Palffy-Muhoray, B. Taheri, Tunable mirrorless lasing in cholesteric liquid crystalline elastomers, *Adv. Mater.* 13 (2001), [https://doi.org/10.1002/1521-4095\(200107\)13:14<1069::AID-ADMA1069>3.0.CO;2-6](https://doi.org/10.1002/1521-4095(200107)13:14<1069::AID-ADMA1069>3.0.CO;2-6).
- [3] J.P. Dowling, M. Scalora, M.J. Bloemer, C.M. Bowden, The photonic band edge laser: a new approach to gain enhancement, *J. Appl. Phys.* 75 (1994) 1896–1899, <https://doi.org/10.1063/1.356336>.
- [4] H. Coles, S. Morris, Liquid-crystal lasers, *Nat. Photonics* 4 (10) (2010) 676–685, <https://doi.org/10.1038/nphoton.2010.184>.
- [5] T. Ali, J. De Lin, B. Snow, X. Wang, S.J. Elston, S.M. Morris, A Thin-film flexible defect-mode laser, *Adv. Opt. Mater.* 8 (2020), <https://doi.org/10.1002/adom.201901891>.
- [6] K. Funamoto, M. Ozaki, K. Yoshino, Discontinuous shift of lasing wavelength with temperature in cholesteric liquid crystal, *Jpn. J. Appl. Phys. Part 2: Lett.* 42 (2003), <https://doi.org/10.1143/jjap.42.11523>.
- [7] S. Furumi, S. Yokoyama, A. Otomo, S. Mashiko, Electrical control of the structure and lasing in chiral photonic band-gap liquid crystals, *Appl. Phys. Lett.* 82 (1) (2003) 16–18, <https://doi.org/10.1063/1.1534613>.
- [8] R.R. Gattass, E. Mazur, Femtosecond laser micromachining in transparent materials, *Nat. Photonics* 2 (4) (2008) 219–225, <https://doi.org/10.1038/nphoton.2008.47>.
- [9] K.C. Neuman, S.M. Block, Optical trapping, *Rev. Sci. Instrum.* 75 (9) (2004) 2787–2809, <https://doi.org/10.1063/1.1785844>.
- [10] T. Koonen, F. Gomez-Agis, F. Huijskens, K.A. Mekonnen, Z. Cao, E. Tangdiongga, High-capacity optical wireless communication using two-dimensional IR beam steering, *J. Lightwave Technol.* 36 (19) (2018) 4486–4493, <https://doi.org/10.1109/JLT.2018.2834374>.
- [11] Z. He, F. Gou, R. Chen, K. Yin, T. Zhan, S.T. Wu, Liquid crystal beam steering devices: principles, recent advances, and future developments, *Crystals (Basel)* 9 (2019), <https://doi.org/10.3390/cryst9060292>.
- [12] J. Stockley, S. Serati, Advances in liquid crystal beam steering, in: *Free-Space Laser Communications IV*, SPIE, 2004, p. 32, doi: 10.1117/12.562595.
- [13] R.J. Bussjager, J.M. Osman, Q.W. Song, X.-M. Wang, Design of PLZT electro-optic beam-steering device, in: A.R. Pirich (Ed.), 1996, p. 90, doi: 10.1117/12.243092.
- [14] V.V. Nikulin, Modeling of an acousto-optic laser beam steering system intended for satellite communication, *Opt. Eng.* 40 (2001) 2208, <https://doi.org/10.1117/1.1403022>.
- [15] L. Ge, M. Duelli, R.W. Cohn, Enumeration of illumination and scanning modes from real-time spatial light modulators, *Opt. Express* 7 (2000), <https://doi.org/10.1364/OE.7.000403>.
- [16] J. Kim, M.N. Miskiewicz, S. Serati, M.J. Escuti, Demonstration of large-angle nonmechanical laser beam steering based on LC polymer polarization gratings, in: W.E. Thompson, P.F. McManamon (Eds.), 2011, p. 80520T, <https://doi.org/10.1117/12.886508>.
- [17] J. Kim, C. Oh, S. Serati, M.J. Escuti, Wide-angle, nonmechanical beam steering with high throughput utilizing polarization gratings, *Appl. Opt.* 50 (2011) 2636, <https://doi.org/10.1364/AO.50.002636>.
- [18] C. Oh, J. Kim, J. Muth, S. Serati, M.J. Escuti, High-throughput continuous beam steering using rotating polarization gratings, *IEEE Photonics Technol. Lett.* 22 (4) (2010) 200–202, <https://doi.org/10.1109/LPT.2009.2037155>.
- [19] J. Kim, C. Oh, M.J. Escuti, L. Hosting, S. Serati, Wide-angle nonmechanical beam steering using thin liquid crystal polarization gratings, in: J.D. Goglewski, R.A. Carreras, T.A. Rhoadarmer (Eds.), 2008, p. 709302, <https://doi.org/10.1117/12.795752>.
- [20] S.Y. Cho, H. Yoshida, M. Ozaki, Emission direction-tunable liquid crystal laser, *Adv. Opt. Mater.* 8 (2020) 1–6, <https://doi.org/10.1002/adom.202000375>.
- [21] J. Kobashi, Y. Mohri, H. Yoshida, M. Ozaki, Circularly-polarized, large-angle reflective deflectors based on periodically patterned cholesteric liquid crystals, *Optical Data Processing Storage 3* (2017), <https://doi.org/10.1515/odps-2017-0008>.
- [22] M. Ivanov, T. Eiju, Compact spectral ellipsometer with polarization grating, in: *Optoelectronics, Materials, and Devices for Communications*, SPIE, 2001, p. 664, <https://doi.org/10.1117/12.444941>.
- [23] C.F. LaCasse, B.J. Redman, M.W. Kudenov, J.M. Craven, Maximum bandwidth snapshot channelled imaging polarimeter with polarization gratings, in: *Polarization: Measurement, Analysis, and Remote Sensing XII*, SPIE, 2016, p. 98530U, <https://doi.org/10.1117/12.2228561>.
- [24] M.W. Kudenov, M.N. Miskiewicz, M.J. Escuti, J. Coward, Compact spatial heterodyne interferometer using polarization gratings, in: *Polarization Science and Remote Sensing VI*, SPIE, 2013, p. 88730Q, <https://doi.org/10.1117/12.2024104>.
- [25] G. Cincotti, G. Costa, Polarization grating-based wavelength selective switches, in: 2016 18th International Conference on Transparent Optical Networks (ICTON), IEEE, 2016, <https://doi.org/10.1109/ICTON.2016.7550564>.
- [26] G. Cincotti, Polarization gratings: design and applications, *IEEE J. Quantum Electron.* 39 (12) (2003) 1645–1652, <https://doi.org/10.1109/JQE.2003.819526>.
- [27] J. Kim, M.N. Miskiewicz, S. Serati, M.J. Escuti, Nonmechanical laser beam steering based on polymer polarization gratings: design optimization and demonstration, *J. Lightwave Technol.* 33 (10) (2015) 2068–2077, <https://doi.org/10.1109/JLT.2015.2392694>.
- [28] Z. Wang, C. Wang, S. Liang, X. Liu, Diffraction characteristics of a non-mechanical beam steering system with liquid crystal polarization gratings, *Opt. Express* 30 (2022) 7319, <https://doi.org/10.1364/OE.452397>.
- [29] Z.-W. Zhao, C.-M. Wang, S.-Z. Li, W. Chen, Y.-G. Liu, Q.-Q. Mu, Z.-H. Peng, Q.-D. Wang, L. Xuan, R.-D. Wei, High-efficiency large-angle reflective composite polarization grating, *Liq. Cryst.* 47 (2) (2020) 191–198, <https://doi.org/10.1080/02678292.2019.1633584>.
- [30] C.-J. Yu, J. Kim, D.-W. Kim, S.-D. Lee, Polarization grating of photoaligned liquid crystals with oppositely twisted domain structures, *Mol. Cryst. Liq. Cryst.* 433 (1) (2005) 175–181, <https://doi.org/10.1080/15421400590955000>.
- [31] T. Sasaki, H. Ono, N. Kawatsuki, Functionalized polarization gratings in AZO-dye doped polymer films, *Mol. Cryst. Liq. Cryst.* 472 (2007) 131/[521]–136/[526], <https://doi.org/10.1080/15421400701545312>.
- [32] C. Mowatt, S.M. Morris, M.H. Song, T.D. Wilkinson, R.H. Friend, H.J. Coles, Comparison of the performance of photonic band-edge liquid crystal lasers using different dyes as the gain medium, *J. Appl. Phys.* 107 (2010), <https://doi.org/10.1063/1.3284939>.
- [33] S.M. Morris, A.D. Ford, C. Gillespie, M.N. Pivnenko, O. Haderl, H.J. Coles, The emission characteristics of liquid-crystal lasers, *J. Soc. Inf. Disp.* 14 (2006), <https://doi.org/10.1889/1.2210808>.
- [34] W. Cao, P. Palffy-Muhoray, B. Taheri, A. Marino, G. Abbate, Lasing thresholds of cholesteric liquid crystals lasers, in: *Molecular Crystals and Liquid Crystals*, 2005, pp. 101–110, <https://doi.org/10.1080/15421400590930782>.
- [35] T.M. Sarukhanyan, The polarization of laser generation from the cholesteric liquid crystal–dye-doped polymer layer-cholesteric liquid crystal system, *J. Contemp. Phys.* 56 (2) (2021) 103–108, <https://doi.org/10.3103/S1068337221020146>.
- [36] X. Zhan, F. Xu, Z. Zhou, Y. Yan, J. Yao, Y.S. Zhao, 3D laser displays based on circularly polarized lasing from cholesteric liquid crystal arrays, *Adv. Mater.* (2021), <https://doi.org/10.1002/adma.202104418>.
- [37] Z. He, Y.-H. Lee, K. Yin, S.-T. Wu, Recent advances in liquid-crystal polarization volume gratings, in: I.C. Khoo (Ed.), *Liquid Crystals XXIII*, SPIE, 2019, <https://doi.org/10.1117/12.2527787>.
- [38] Y. Jin, S.J. Elston, J.A.J. Fells, M.J. Booth, C. Welch, G.H. Mehl, S.M. Morris, Millisecond optical phase modulation using multipass configurations with liquid-crystal devices, *Phys. Rev. Appl.* 14 (2020), <https://doi.org/10.1103/PhysRevApplied.14.024007>.